Оптический журнал

Оптическое приборостроение

Side polished graded index multimode fiber based refractive index sensor for biology measurement

© 2018 г. Dan Gao*, **; Hao Lei**, ***; Jun Zhang**, ***; Jianhui Yu**, ***; Wenguo Zhu**, ***; Huihui Lu**, ***; Heyuan Guan**, ***; Jieyuan Tang**, ***; Mengyuan Xie**, ***; Yunhan Luo**, ***; Jiangli Dong**, ***; Norhaha Arsad****; Zhe Chen**, ***; Fan Wang*

*School of Mechanics and Construction Engineering, Jinan University, Guangzhou 510632, China
**Guangdong Provincial Key Laboratory of Optical Fiber Sensing and Communications, Jinan University, Guangzhou 510632, China
***Key Laboratory of Optoelectronic Information and Sensing Technologies of Guangdong Higher Education Institutes, Jinan University, Guangzhou 510632, China
****Centre for Advanced Electronics & Communication Engineering, Faculty of Engineering and Built Environment, Universiti Kebangsaan Malaysia, 43600 UKM Bangi, Selangor Malaysia

E-mail: 472969511@qq.com

Поступила в редакцию 05.06.2018

DOI:10.17586/1023-5086-2018-85-12-49-59

A side polished graded index multimode fiber based refractive index sensor is proposed for use in biology measurement. The side polished graded index multimode fiber is fabricated using the wheel polishing method, that is a part of the cladding and core of a graded index multimode fiber are removed to develop a leaking 'window' called side polished region. The optical power loss through this structure is sensitive to the refractive index of the analyte liquid which covering the leaking 'window'. A greatly linear correlation between the optical power loss and refractive index has been achieved. Additionally, we also investigated the influence of each structure parameter on the sensitivity and linearity. From simulation and experiments results obtained, the fiber core of 50 μm and R of 10 μm are considered as the best choice of fiber structure with its sensitivity is 40.92 dB/RIU in the refractive index range of 1.300–1.450. A bio-solution of fetal bovine serum can be easily detected with this structure whose concentration gradient is two percent. It provides a simple and quick method to detect refractive indices in biology measurement from 1.300 to 1.450. .

Keywords: *side polished graded index multimode fiber, refractive index sensor, biological measurement, optical power loss.*

OCIS codes: *060.0060.*

Датчик для измерения показателя преломления на основе градиентного многомодового волокна с полированной боковой поверхностью для биологических применений

© 2018 г. Dan Gao, Hao Lei, Jun Zhang, Jianhui Yu, Wenguo Zhu, Huihui Lu, Heyuan Guan, Jieyuan Tang, Mengyuan Xie, Yunhan Luo, Jiangli Dong, Norhaha Arsad, Zhe Chen, Fan Wang

Предложен датчик на основе градиентного многомодового волокна с полированной боковой поверхностью для измерения показателя преломления в биологических исследованиях. Часть боковой поверхности волокна, включая оболочку и часть сердцевины, механически сполировывалась так, чтобы организовать окно утечки излучения. Потери мощности из волокна при этом чувствительны к величине показателя преломления жидкостей, определяемых при анализе и контактирующих с окном утечки. Обнаружена корреляция высокой степени линейности между потерями и величиной показателя преломления аналита.

Исследовано влияние каждого из параметров изготовленной структуры на чувствительность и линейность при проведении измерений. Моделирование и эксперимент показали, что наилучшие результаты демонстрирует волокно с диаметром сердцевины 50 мкм и расстоянием от её оси до площадки утечки 10 мкм, обеспечивая чувствительность 40,92 дБ на единицу изменения показателя преломления в диапазоне 1,300–1,450 мкм. С лёгкостью обнаруживались двухпроцентные изменения показателя преломления в коровьей внутриутробной сыворотке. Обеспечивается простое и быстрое определение показателей преломления в области 1,3–1,45 мкм при проведении биологических исследований. .

Ключевые слова: *многомодовое градиентное оптическое волокно, полированная боковая поверхность, уходящие волны, датчик на основе градиентного волокна, биологические измерения.*

1. INTRODUCTION

Biological tissue refractive index (RI) is an important biophysics parameter correlated with other biophysics properties including electrical and optical properties. It represents not only the intracellular mass and concentration of a cell, but also provides an important insight into various biological models [1].

Biological tissue RI measurement has been extensively studied and measured since the 1950s, and played an important role in various detection and diagnosis. As an important branch, the study of optical fiber based on the RI sensor has been getting increasingly extensive due to its advantages, such as simple construction, compactness, ease of use, immunity to electromagnetic waves, potential for remote operation, and flexibility of directly embedding into a different system, etc. There are a number of optical fiber RI sensors based on both the single mode fiber and the multimode fiber [2–4], including long-period fiber grating [5–10], fiber Bragg grating [11–15], Fabry–Perot interferometer and Mach–Zehnder interferometer [16–20], macro-bend single mode fiber [21], surface plasmon resonance, Single Mode–Multimode–Single Mode fiber [22], etc. However, all of above optical fiber RI sensors require precision devices and complex methods to improve detection resolution, and their RI sensitivities at the working range of 1.300–1.330 are not high.

Previous investigations showed that multimode fiber has been identified as a good sensing medium which a variety of sensors had been based on [14], [23–26]. More and more studies now focus on the graded index multimode fiber (GIMMF) rather than step index multimode fiber (SIMMF) for its better transmission characteristics. The fiber side polishing technology has been proven to be an easy and effective method which is applied in lots of RI sensors [27]. Thus, combining the GIMMF and the fiber side polishing technology can increase the sensitivity and working range for the biological tissue RI measurement and is easy to manufacture. Through the wheel polishing method, forming a polished region in the graded index multimode fiber will lead to an optical power loss during light propagation. So that, the side polished graded index multimode fiber (SPGIMMF) would be a better transducer element, and the optical power loss is decided by structural parameters and analyte RI. A side polished graded index multimode fiber structure based sensor has the additional advantages of low cost and ease of fabrication while being well-behave in the entire biological tissue RI interval.

2. SIDE POLISHED GRADED INDEX MULTIMODE FIBER

2.1. Configuration of side polished graded index multimode fiber

The configuration of the side polished graded index multimode fiber is shown in Fig. 1. A part of the cladding and core of the graded index multimode fiber is removed, which develops into a leaking 'window' called a side polished region as indicated as L_0, a total length of this 'window'. This 'window' consists of a flat and two curved surfaces called the flat

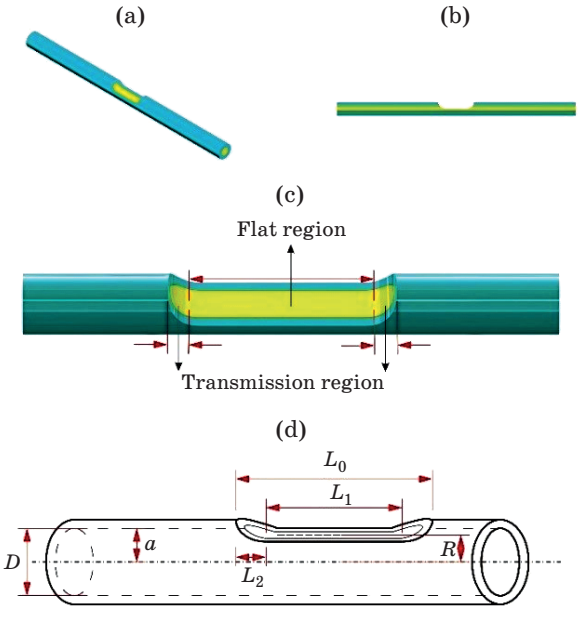

Fig. 1. The side polished graded index multimode fiber. The contour and the cross profile of the side polished graded index multimode fiber (a–b). The flat region and transmission region in the polished area (c). Vertical section with main parameters marked (d).

region as indicated by L_1 and a transmission region as indicated by L_2. Meanwhile, R is used to indicate the residual radius which stands for the minimum distance between the polished region and the center of the multimode fiber. In addition, D indicates the diameter of the graded index multimode fiber core, while a is the radius of fiber [28].

2.2. The working principle of side polished graded index multimode fiber

When light is launched from one end of the fiber, the light is fully reflected at the interface of the core and cladding, so that the light passes almost without any loss output to the other end of the fiber. The leaking "window" of the SPGIMMF is made by the wheel polishing method. Changing the environment of the leaking "window" or the parameters of the SPGIMMF will influence the optical field distribution in the MMF. As a result, the output spectrum or the optical power of the MMF will be changed based on RI of the biological tissue liquid filling the side polished region, the biological tissue RI is measured by the change of the output spectrum or the optical power of the MMF.

3. FABRICATION OF SIDE POLISHED GRADED INDEX MULTIMODE FIBER

We conducted three groups of experiments with different structures of SPGIMMF according to table 1 using the wheel polishing method. Fiber wheel polishing method refers to the optical fiber being placed at the edge of a rotating polishing wheel, touching it. The wheel, which exerts an axial tension, will polish away a part of the fiber cladding when it rotates [28]. Group A and Group B utilized fibers

Table 1. Parameters of the SPGIMMF model in simulation

Parameters	Values		
Light wavelength	1310 nm		
Total length of fiber	20 cm		
Total length of SPGIMMF structure	2 cm		
Length of flat region	1.8 cm		
Length of transition region	0.1×2 cm		
Group	A	B	C
Fiber diameter	125 μm	125 μm	125 μm
Core diameter	50 μm	62.5 μm	105 μm
R, μm	0	0	10
	10	10	20
	20	20	30
	25	30	50

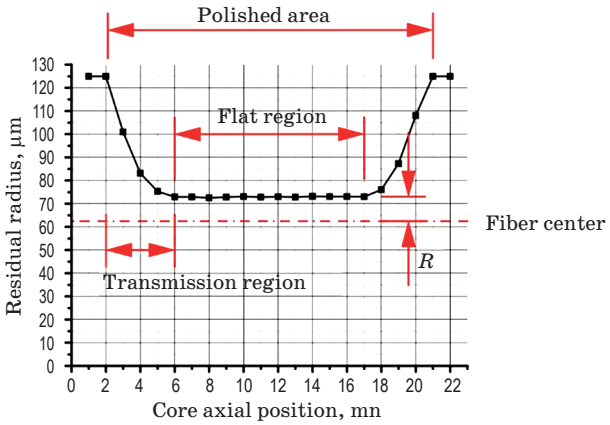

Fig. 2. Measurement of residual radius R.

of different core diameter from the same company, YOFC 50/125-OM2 (D = 50 μm) and YOFC 62.5/125-OM1 (D = 62.5 μm). The last group, Group C applied Nufern MM-S105/125-22A with a fiber core diameter of 105 μm. First, the two flat fiber optic fixtures are respectively fixed on the optical fiber fixture table. After that, a little bit of the coating layer of optical fiber due to be polished is removed. Fix the optical fiber on the fixture after straightening, then move the polishing wheel so that the abrasive paper of the grinding wheel is just located above the position of no cladding optical fiber. The tension control system is used to ensure the optical fiber clamp horizontally while moving on the guide rail to exert a tensile force on the optical fiber axis. Subsequently, the lifting and lowering motor will move the polishing wheel downward until the abrasive paper contacts the optical fiber. The tensile force at this time must remain the set value in the tension testing system. The motor then rotates the polishing wheel to start polishing. To determine whether the fiber side polishing is complete, the optical power value of the optical fiber can be checked to see whether it meets the requirements yet. When the optical power reaches the predetermined value, the polishing is complete.

After fabrication, R was measured by using a microscope. The measured results of R are close to the designed figures. One of the results is in Fig. 2 shown R of 10 μm on the side of polished graded index multimode fiber.

4. NUMERICAL SIMULATION

4.1. Configuration of simulation model

In the simulation, all parameters were set to the real value in Table 1. A total of 20 cm length was set for the whole systems. The length is long enough to get correct result but not take too much computing resource. As for the SPGIMMF structure, SPGIMMF

was set to 2 cm, with the flat region occupying ninety percent of it. Meanwhile, the light wavelength was set at 1310 nm. A launch field was set in the initial position of the fiber, while a monitor of an optical power was used to detect the optical power through the whole system. The model structures and RI profile are shown in Fig. 3.

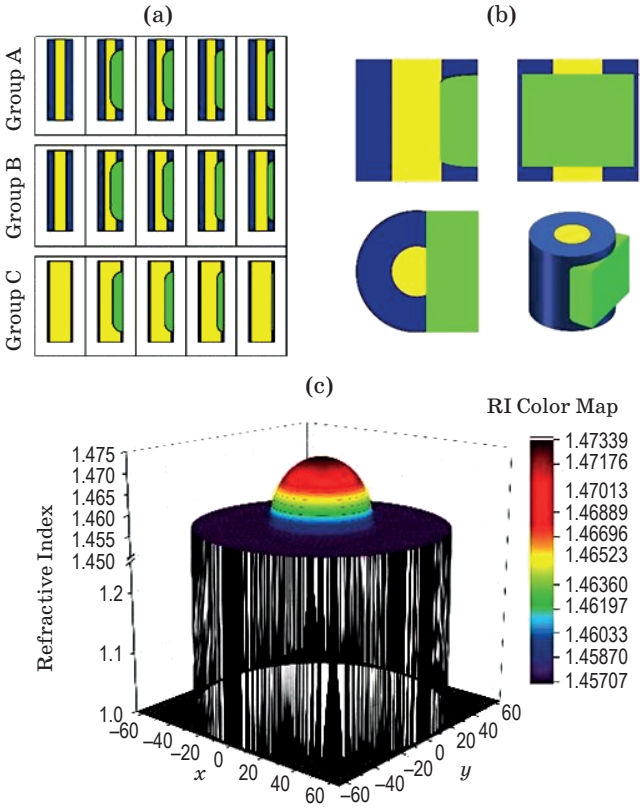

Fig. 3. The model structures and RI profile. Three groups with different core diameter and different R (a), simulation models (b) and the refractive index profile (c).

4.2. Simulation result

We ran three groups of simulation with the structural parameters as shown in table 1 by the method of three dimension finite difference beam propagation. In each simulation, we made the step change of the analyte RI from 1.300 to 1.450 by 0.005. The results are shown in Fig. 4.

As shown in Fig. 4, Group A and Group B both show great linearity from 1.300 to 1.450, wheares Group C with a core diameter of 105 μm also shows a good linearity from 1.300 to 1.410. We found that for the same core diameter, the smaller the R is, the better is the linearity. As the numerical simulation is done in the ideal environment, the optical power loss is smaller than the measured value. The simulation results and linearity of each group is shown in Table 2.

Table 2. Simulation result and Linearity in each group

Group	Workspace (RIU)	D, μm	R, μm	Linearity
A	1.300–1.450	50	0	0.95324
		50	10	0.98172
		50	20	0.93768
		50	25	0.95121
B	1.300–1.450	62.5	0	0.92869
		62.5	10	0.98928
		62.5	20	0.98435
		62.5	30	0.96779
C	1.300–1.410	105	10	0.94372
		105	20	0.96288
		105	30	0.97456
		105	50	0.97744

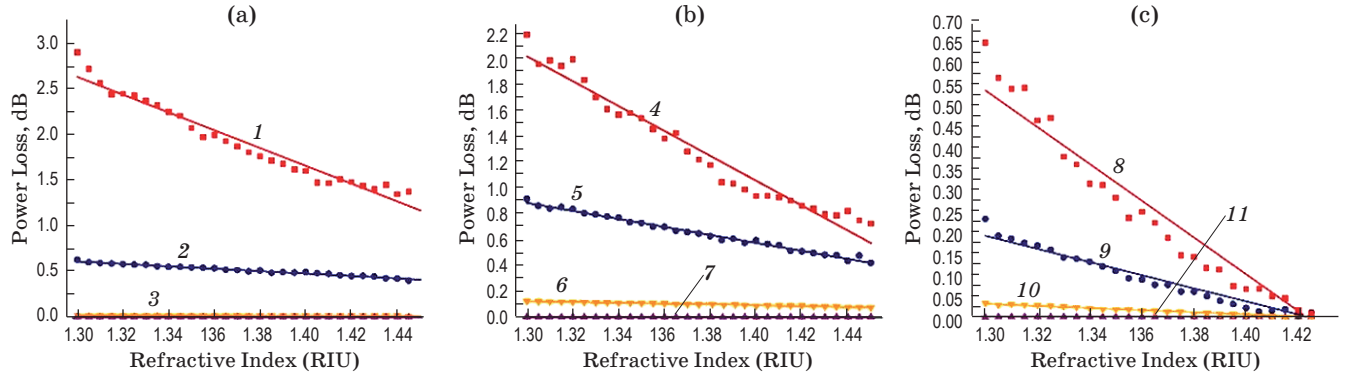

Fig. 4. The results of three groups of simulation by the method of three dimension finite difference beam propagation. Group A and Group B with core diameters of 50 μm and 62.5 μm show great linearity with different R from 1.300 to 1.450 (*1* — $D = 50.0$ μm, $R = 0$ μm, *2* — $D = 50.0$ μm, $R = 10$ μm, *3* — $D = 50.0$ μm, $R = 20$ μm, $D = 50.0$ μm, $R = 25$ μm, *4* — $D = 62.5$ μm, $R = 0$ μm, *5* — $D = 62.5$ μm, $R = 10$ μm, *6* — $D = 62.5$ μm, $R = 20$ μm, *7* — $D = 62.5$ μm, $R = 30$ μm) (a—b). Group C with a core diameter of 105 μm shows great linearity with different R from 1.300 to 1.410 (*8* — $D = 105.0$ μm, $R = 10$ μm, *9* — $D = 105.0$ μm, $R = 20$ μm, *10* — $D = 105.0$ μm, $R = 30$ μm, *11* — $D = 105.0$ μm, $R = 50$ μm) (c).

Clearly, good linearity in every simulation run proved that this structure is a reliable one, with different R leading to different sensitivity. But this is the ideal result, the actual performance of this structure will be explored by a series of experiments.

5. EXPERIMENT AND RESULT

5.1. Experiment setup

Figure 5a schematically illustrates the experiment setup used to investigate the sensing characteristics of the SPGIMMF with different sizes of core diameters and different values of R. A 1310 nm wavelength of optical power source is connected to a 1×2 optical fiber coupler. The optical coupler is split into two: one to the SPGIMMF and an optical power meter with 0.001 dB resolution for output measurement, whereas the other one is direct to another optical power meter which acts as a reference. Optical power loss is monitored to observe the behavior of the SPGIMMF when the RI liquid is applied. Figure 5b is a zoom-in of the SPGIMMF structure that used in the experiment.

5.2. Spectrum of SPGIMMF

To explore spectrum characteristics of the SPGIMMF, two different group of spectra are measured by using an optical spectrum analyzer with 0.01 nm. Resolution is used to observe the output spectra as shown in Fig. 6.

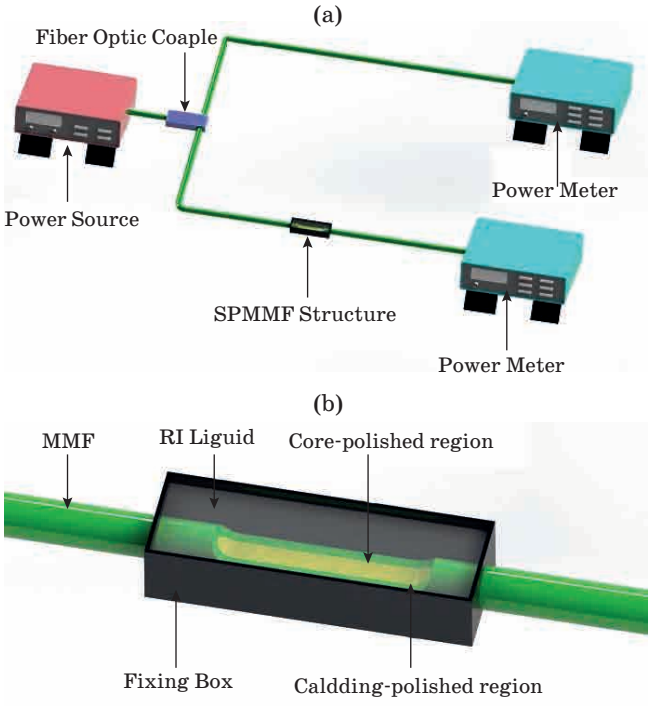

Fig. 5. The experiment setup. The experimental setup (a), the structure of the SPGIMMF (b).

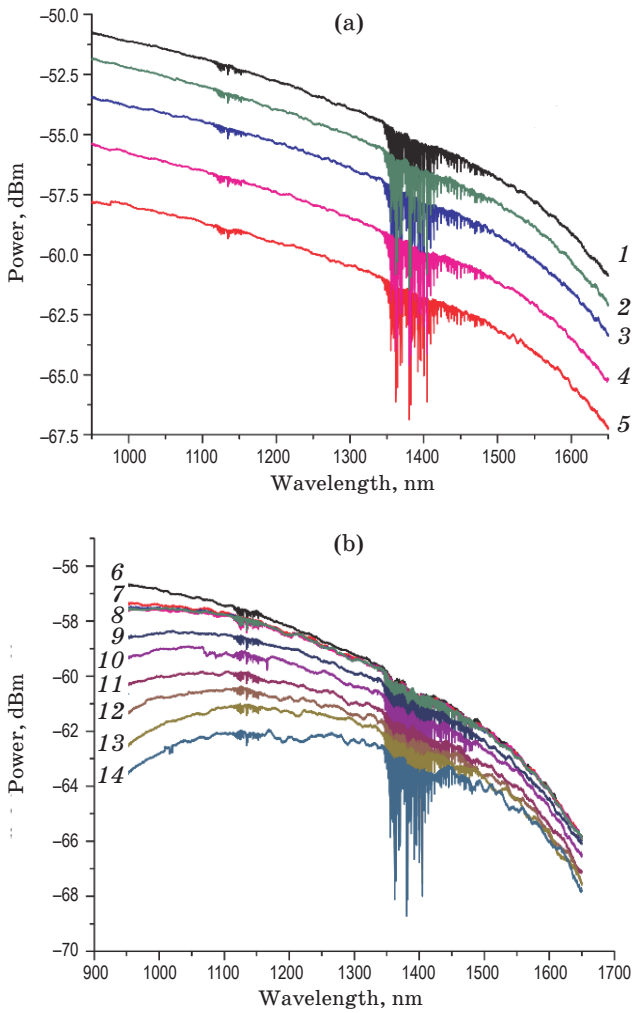

Fig. 6. Spectra of the SPGIMMF. Spectra characteristics of Group A with different R (*1* — light source, *2* — 25 μm, *3* — 20 μm, *4* — 10 μm, *5* — 0 μm) lead to different optical power loss of the same shape (a). Spectra of different RI (*6* — light source, *7* — 1.450,*8* — 1.430, 1.410, 1.390, *9* — 1.375, *10* — 1.360, *11*— 1.345, *12* — 1.330, *13* — 1.315, *14* — 1.300) liquids show the same tendency and little difference (b).

Figure 6a is the spectra of Group A. Obviously, with different light sources, the four spectra are similar only in shape. In other words, this structure does not lead to any wavelength selectivity but the optical power loss.

Then, as for the influence of different RI liquids on the spectrum, the SPGIMMF with a core diameter of 50 μm and R of 10 μm, was tested, with its polished area covered by standard RI liquid the result is shown in Fig. 6b. Although the spectra of different RI liquids are not exactly the same, they showed the same tendency.

Figure 7 showed that there is a greatly linear relationship between RI of cover liquid and optical power loss during a specific RI interval. In Group A and Group B, the linear relationship is continuous from 1.300 to 1.450 while Group C behaves comparably

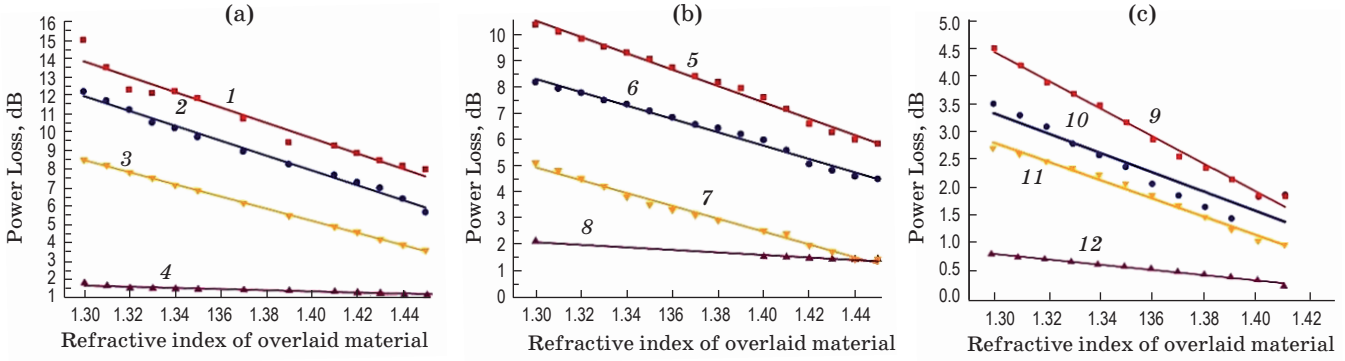

Fig. 7. Different R leads to different sensitivity. Group A and Group B with core diameters of 50 μm and 62.5 μm show great linearity with different R from 1.300 to 1.450 (*1* — $D = 50.0$ μm, $R = 0$ μm, *2* — $D = 50.0$ μm, $R = 10$ μm, *3* — $D = 50.0$ μm, $R = 20$ μm, *4* — $D = 50.0$ μm, $R = 25$ μm, *5* — $D = 62.5$ μm, $R = 0$ μm, *6* — $D = 62.5$ μm, $R = 10$ μm, *7* — $D = 62.5$ μm, $R = 20$ μm, *8* — $D = 62.5$ μm, $R = 30$ μm) (a—b). Group C with a core diameter of 105 μm shows great linearity with different R from 1.300 to 1.410 (*9* — $D = 105.0$ μm, $R = 10$ μm, *10* — $D = 105.0$ μm, $R = 20$ μm, *11* — $D = 105.0$ μm, $R = 30$ μm, *12* — $D = 105.0$ μm, $R = 50$ μm) (c).

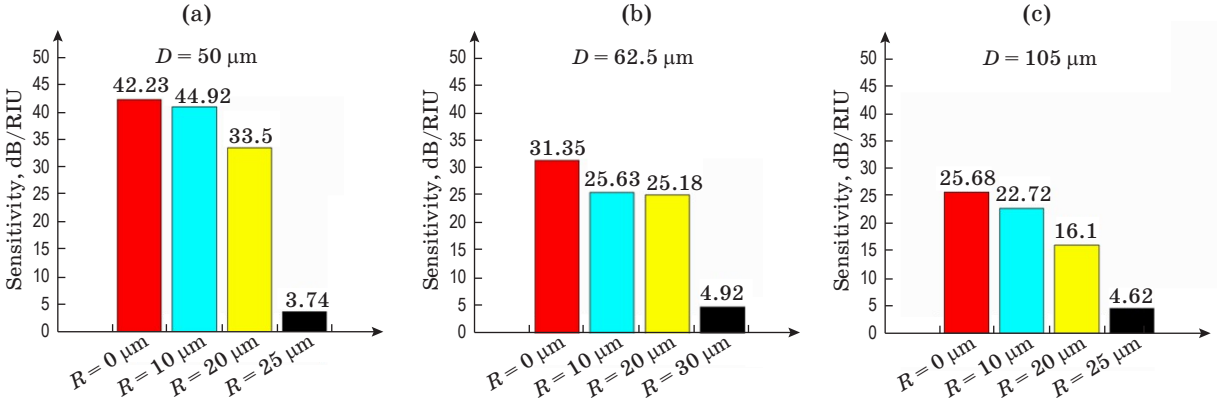

Fig. 8. Sensitivity of different groups.

during 1.300–1.410. Similar to the results of the previous simulation, the experiment exhibits the same trend. In actual measurement, the polishing surface is not absolutely smooth, thus there is a slight deviation between the measured and the simulation values. As the numerical simulation is conducted in the ideal environment, thus, the optical power loss is lower than the measured value. And the curvilinear trend in the figure shows that the optical power loss decreases with the increase of the standard liquid RI (The liquid RI is known).

The linearity of each groups of the SPGIMMF is shown in Table 3. From the table, we observed that the SPGIMMF is highly sensitive and reliable with only one is less that 0.95 of linearity while others are larger than it due to polishing surface. It is because the higher the linearity, the smaller the fluctuation of the optical power loss with the refractive index, and the more accurate the refractive index of the measured biological tissue fluid will be.

On this basis, we found that the sensitivity, namely the fitting curve slope which shows the magnitude of light loss caused by the RI change. Hence, different structure parameters gave different sensitivity as shown in Fig. 8.

Table 3. Linearity of three groups of the SPGIMMF

Group	Workspace (RIU)	D, μm	R, μm	Linearity
A	1.300–1.450	50	0	0.956
		50	10	0.992
		50	20	0.999
		50	25	0.931
B	1.300–1.450	62.5	0	0.991
		62.5	10	0.988
		62.5	20	0.990
		62.5	30	0.954
C	1.300–1.410	105	10	0.997
		105	20	0.998
		105	30	0.986
		105	50	0.988

As Fig. 7 has shown, when the fiber core diameter is fixed, the optical power loss increases with the

decrease of R. To check whether the trend is acceptable, we placed a different R in air and measured the transmittance of optical power with the change of R.

Figure 9 shows that when the polished area of the SPGIMMF is exposed to air, the overall trend of the curve is that the transmittance of the optical power increases with the increase of R, which translates to the decrease of optical power loss decreases. However, the curve also has a small float in the process of rising. From Fig. 9, it can be concluded that when R is 0 μm, the maximum power loss is achieved. When R is 10 μm, the curve has a trough, and the optical power loss is close to the optical power loss when R is 0 μm. And when R is fixed, the relationship between the optical power loss and the fiber core diameter is shown in Fig. 10. It can be understood that the optical power loss increases with the decrease of the fiber core diameter.

5.3. Discussion

The SPGIMMF is investigated both in simulation and experimental for its sensing characteristics. Three types of SPGIMMF structures with different sizes of core diameter and R namely group A, B and C are conducted with different standard of RI liquid. The results show the structure would affect the optical power loss rather than causing wavelength selectivity. The relationship between analyte RI and optical power loss with the SPGIMMF structure has been explored through experimentation. Group A and Group B fibers with core diameters of 50 μm and 62.5 μm show great linearity with different R from 1.300 to 1.450 while Group C fibers with core diameters of 105 μm shows great linearity with different R from 1.300 to 1.410. When the diameter of the SPGIMMF and R are invariants, the optical power loss decreases with the increase of the standard liquid RI. When the diameter of the SPGIMMF and the standard liquid RI are invariants, the optical power loss decreases with the increase of R, and the minimum value is obtained when R is 0 μm or 10 μm. When the standard liquid RI and the R are invariants, the optical power loss decreases with the increase of the diameter of the SPGIMMF. The larger optical power loss is, the easier for the sensor to detect. The linearity of R for 10 μm is better than that of R for 0 μm, but the SPGIMMF is easier to be damaged when R is too small. Thus, we concluded that at diameter of 50 μm and an R value of 10 μm is the best choice for this SPGIMMF structure. The specific sensitivity is determined by the kind of MMF and fabrication parameters. With the best parameters, the SPGIMMF sensor can achieve at sensitivity of 40.92 dB/RIU.

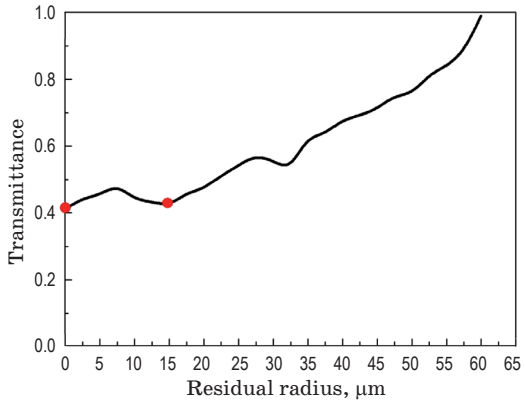

Fig. 9. The relationship between transmittance of optical power and R.

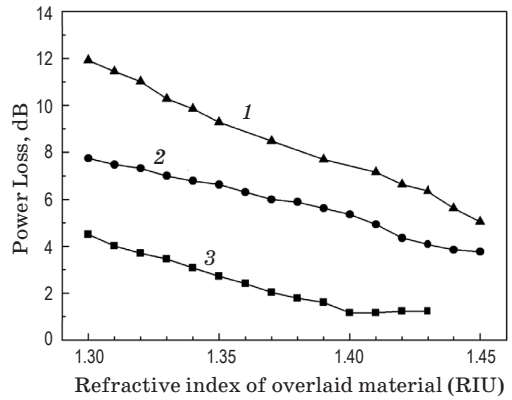

Fig. 10. The relationship between optical power loss and the standard liquid RI in different SPGIMMF core diameters (*1* — 105.0 μm, *2* — 62.5 μm, *3* — 50.0 μm) for R is 10 μm.

6. SPGIMMF IN BIOMEDICAL APPLICATION

In this section, an experiment was carried out to utilize the SPGIMMF sensor parameters ($D = 50$ μm, $R = 10$ μm) to detect its practicability in biology measurement. Fetal bovine serum (FBS) plays a vital role in bio-culture solutions, whose concentration is an essential parameter. The bio-culture solution with different concentration of FBS will get different composition and different RI. It is unknown whether this sensor can make out this tiny distinction and quantify the solutions or not.

Six bio-culture solutions with FBS concentration from 0% to 10% in the interval of 2% were prepared in advanced as shown in Fig. 11 at NIR wavelengths. Visually, the difference is virtually distinguishable to human eyes. Thus the SPGIMMF sensor is used and the results for each samples are shown in Table 4. (Notes: optical loss is measured by the optical power meter and RI is measured by refractometer).

Table 4. Optical power loss of each bio-culture solution

Concentration	0%	2%	4%	6%	8%	10%
RI	1.3346	1.3350	1.3353	1.3355	1.3356	1.3357
Power loss	12.483	12.464	12.452	12.444	12.439	12.434

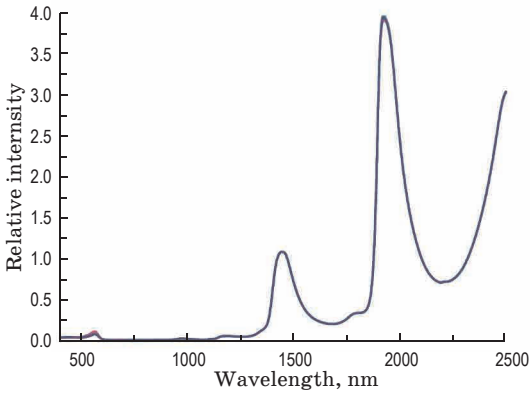

Fig. 11. NIR of each bio-culture solution.

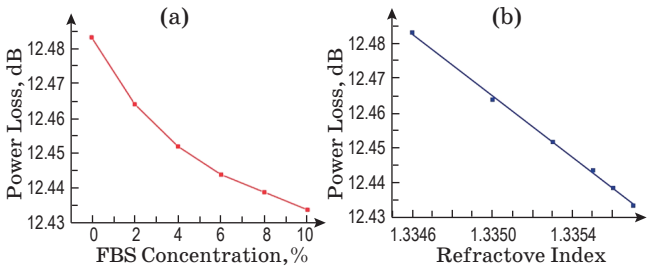

Fig. 12. Optical power loss vs the concentration and refractive index of the FBS solution.

As shown in Fig. 12, an FBS concentration gradient of 2% can be easily detected with the SPGIMMF based sensor and the optical power meter. We found that, a great linearity of the optical power loss and FBS refractive index.

Certainly, when the optical power meter with higher resolution is available, the measurement ought to be easier. As the same with the experiment above, we have nothing by using near infrared spectroscopy. So the biological tissue RI is measurement by the change of the optical power of the SPGIMMF.

7. CONCLUSION

After being fabricated by a wheel polishing method, a SPGIMMF based on RI sensor demonstrated a great performance for its linear response in a specific RI interval. The influence of core diameter and R on this sensor was studied. The results show that smaller R and core diameter will lead to higher sensitivity while other parameters are kept the same. Each SPGIMMF with different core diameters and R has high linearity, which demonstrates it is a reliable method. Considering the linearity, sensitivity and stability of the device, the SPGIMMF with a core diameter of 50 μm and R value of 10 μm is found to be the best choice. This provided a sensitivity of 40.92 dB/RIU in the refractive index range of 1.300–1.450. An FBS concentration gradient of 2% can be easily detected with this SPGIMMF based sensor. It provides a simple and quick method to measure the refractive index of biological material.

8. APPENDIX

As a result of the considerable decrease in modal dispersion, most multimode fibers (MMF) are graded index and weakly guiding fiber whose core has a refractive index that decreases with increasing radial distance from the optical axis of the fiber and approximates the cladding refractive index. The most common RI profile for a graded index multimode fiber is nearly parabolic to refocus the rays in the core and minimize modal dispersion.

When the core closer to the fiber axis that have a higher refractive index than the cladding, lights propagate sinusoidal through the fiber. The most common refractive index profile is very close to parabolic curve as shown in Fig. 13 and equation (1), where n_1 is the RI of fiber cladding, n_2 is the RI of fiber optical axis, and r is the distance from area to the fiber optical axis.

$$n^2(r) = \begin{cases} n_1^2\left[1-2\Delta(r/a)^2\right], r \le a \\ n_2^2 \qquad\qquad , r > a \end{cases} \tag{1}$$

To get the mode property of the graded index multimode fiber, we solved the wave equation in GIMMF with the WKB approximation to find approximate solutions [29, 30]. In the scalar wave Equation shown in equation (2), ψ is the eigenmode of MMF determined by fiber core diameter, fiber core and cladding RI indices, β is the propagation constant of each eigenmode of the MMF, and **k** is the wave vector.

$$\frac{\partial^2\psi}{\partial r^2} + \frac{1}{r}\frac{\partial\psi}{\partial r} + \frac{1}{r^2}\frac{\partial^2\psi}{\partial\varphi^2} + \left(k^2+\beta^2\right)\psi = 0. \tag{2}$$

For further approximation with TEM wave approximation, we focus on electronic field E_x in the cylindrical coordinate system. The wave Equation in

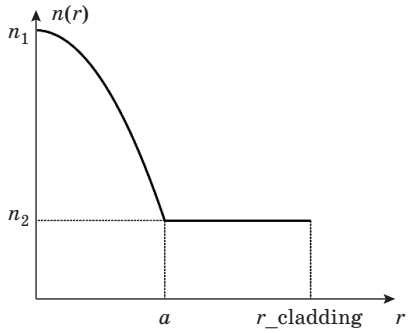

Fig. 13. Refractive index profile of graded index multimode fiber.

the cylindrical coordinate system is shown in equation (3).

$$\frac{\partial^2 E_x}{\partial r^2}+\frac{1}{r}\frac{\partial E_x}{\partial r}+\frac{1}{r^2}\frac{\partial^2 E_x}{\partial \varphi^2}+ \\ +\left(k_0^2 n^2(r)-\beta^2\right)E_x(r,\varphi)=0. \quad (3)$$

In equation (4), we segregate $E_x(r, \varphi)$ into $E(r)$ and $\exp(il\varphi)$ with the segregation variable method, where $E(r)$ indicates the radial intensity of $E_x(r, \varphi)$ and $\exp(il\varphi)$ indicates the phase. Combing equation (3) and equation (4), we get the Equation of $E(r)$ as shown in equation (5).

$$E_x(r,\varphi)=\frac{1}{\sqrt{r}}E(r)\exp(il\varphi), \quad (4)$$

$$\frac{d^2E(r)}{dr^2}+\left[k_0^2n^2(r)-\beta^2-\frac{\left(l^2-\frac{1}{4}\right)}{r^2}\right]E(r)=0. \quad (5)$$

Setting two new parameters M (as show in equation (6)) and $U(r)$ (as show in equation (7)) equation (5) can be simplified to form equation (8).

$$M=k_0^2n_1^2-\beta^2, \quad (6)$$

$$U(r)=\left[k_0^2n_1^2-k_0^2n^2(r)\right]+\frac{\left(l^2-\frac{1}{4}\right)}{r^2}, \quad (7)$$

$$\frac{d^2E(r)}{dr^2}+\left[M-U(r)\right]E(r)=0. \quad (8)$$

The relationship of M and $U(r)$ in the graded index multimode fiber results in specific $E(r)$, namely each specific optical mode. This situation is shown in Fig. 14. Only when $U(r) < M$, can it form the propagation modes rather than evasion modes. Figure 14 (a–c) shows the situations of propagation modes, leaky modes, and radiation modes.

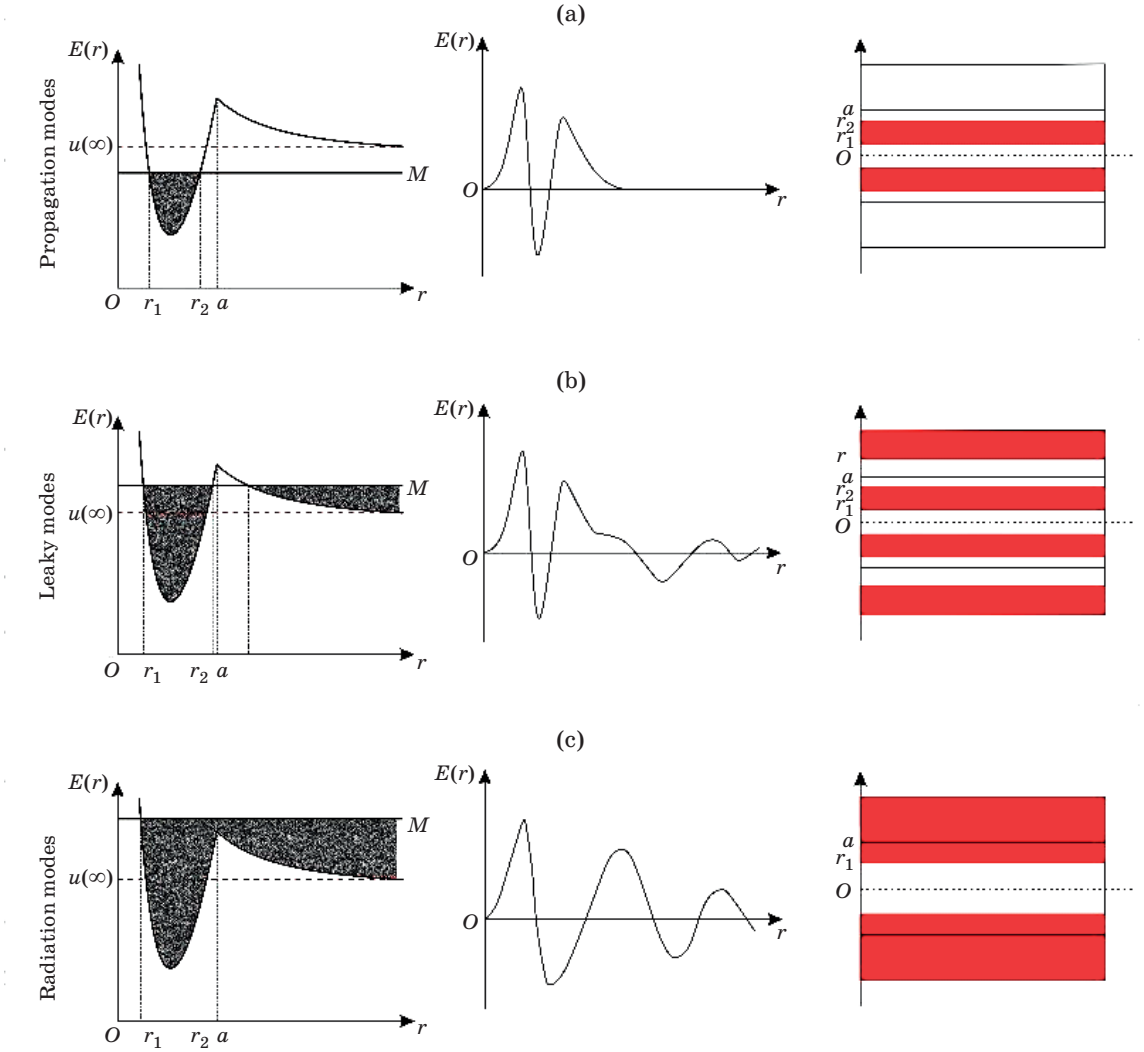

Fig. 14. The Figure shows the relationship of M and $U(r)$. The corresponding $E(r)$ and the area where light modes exist (in red). When $n_2^2k_0^2 < \beta^2 < n_1^2k_0^2$ propagation modes exist in a ring region from r_1 to r_2 (a). When $n_2^2k_0^2 - (l^2 - 1/4)/a^2 < \beta^2 < n_2^2k_0^2$, propagation modes and leaky modes exist at the same time (b). When $\beta^2 < n_2^2k_0^2 - (l^2 - 1/4)/a^2$, only radiation modes exist (c).

Only when the propagation mode is TE or TM, r_1 can be equal to zero. When it comes to the step index fiber, the function $r_2 = a$ will be established.

In the propagation modes, one possible propagation mode in a graded index multimode fiber has been simulated as shown in Fig. 15.

Once a part of cladding and core of multimode fiber is removed and replaced by the analyte liquid, this waveguide structure is essentially destroyed. However, it can be considered that with the decrease of R, more and more light will leak from this 'window'. In the other words, smaller R indicates a bigger window and more optical power loss. Obviously, if only a little cladding and core are wrapped and R is bigger than r_2, it almost does not affect the waveguide structure for most specific modes. Hence, the results of previous simulation and experiments are qualitatively inadvertently.

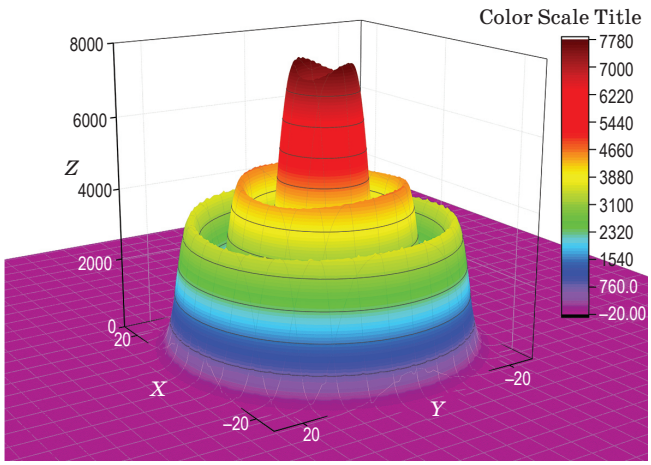

Fig. 15. One propagation mode in a graded index multimode fiber.

This work was supported in parts by National Natural Science Foundation of China (Grant Nos. 61675092, 61475066, 61771222, 61405075, 61401176, 61505069, 61575084); Natural Science Foundation of Guangdong Province (Grant Nos. 2016A030313079, 2014A030313377, 2015A030306046, 2015A030313320, 2016A030311019, 2016A030310098, 2014B010120002); Science and technology projects of Guangdong Province (Grant Nos. 2017A010102006, 2015A020213006, 2015B010125007, 2016B010111003, 2016A010101017); Science & Technology Project of Guangzhou (Grant Nos. 201707010396, 201506010046, 201605030002, 201607010134, 201707010253) and the Fundamental Research Funds for the Central Universities of China (No, 21617333).

REFERENCES

1. *Liu P.Y., Chin L.K., Ser W., Chen H.F., Hsieh C.M., Lee C.H., Sung K.B, Ayi T.C., Yap P.H., Liedberg B., Bourouina T., Leprince-Wang Y.* Cell refractive index for cell biology and disease diagnosis: past, present and future // Lab. Chip. 2016. V. 16. № 4. P. 634–644.
2. *Claudecir R. Biazoli, Susana Silva, Marcos A.R. Franco, Orlando Frazäo, Cristiano M.B. Cordeiro.* Multimode interference tapered fiber refractive index sensors // Appl. Opt. 2012. V. 51. № 24. P. 5941–5945.
3. *Orlando Frazäo, Susana O. Silva, Jaime Viegas, Luís A. Ferreira, Francisco M. Araújo, José L.* Santos. Optical fiber refractometry based on multimode interference // Appl. Opt. 2011. V. 50. № 25. P. E184–E188.
4. *Wenjun Zhou, Yan Zhou, Xxinyong Dong, Li-Yang Shao, Jia Cheng, Jacques Albert.* Fiber-optic curvature sensor based on cladding-mode Bragg grating excited by fiber multimode interferometer // IEEE Photonics J. 2012. V. 4. № 3. P. 1051–1057.
5. *Jin-Fei Ding, Zhang A.P., Li-Yang Shao, Jin-Hua Yan, Sailing He.* Fiber-taper seeded long-period grating pair as a highly sensitive refractive-index sensor// IEEE Photonic Techl. 2005. V. 17. № 6. P. 1247–1249.
6. *Qiu-Shun Li, Xu-Lin Zhang, Dong Xiang, Lan Zheng, Yan Yang, Jun-Hui Yang, Dong Feng, Wen-Fei Dong.* An ultrasensitive long-perios fiber grating-based refractive index sensor with long wavelengths // Sensors. 2016. V. 16. № 12. P. 2205.
7. *Amit Singh.* Various characteristics of long-period fiber grating-based refractive index sensor // Optik. 2015. V. 126. № 24. P. 5439–5543.
8. *Śmietana M., Kova M., Miulic P., Bock W.J.* Measurements of reactive ion etching process effect using long-period fiber gratings // Opt. Express. 2014. V. 22. № 5. P. 5986–5994.
9. *Śmietana M., Kova M., Miulic P., Bock W.J.* Towards refractive index sensitivity of long-period gratings at level of tens of μm per refractive index unit: fiber cladding etching and nano-coating deposition // Opt. Express. 2016. V. 24. № 11. P. 11897–11904.
10. *Jaw-Luen Tang, Jien-Neng Wang.* Chemical sensing sensitivity of long-period grating sensor enhanced by colloidal gold nanoparticles // Sensors. 2008. V. 8. № 1. P. 171–184.
11. *Coradin F.K., Possetti G.R.C., Kamikawachi R.C., Muller M., Fabris J.L.* Etched fiber bragg gratings sensors for water-ethanol mixtures: a comparative study // J. Microw. Optoelectron. Electromagn. Appl. 2010. V. 9. № 2. P. 131–143.
12. *Yang Ran, Long Jin, Li-Peng Sun, Jie Li, Bai-Ou Guan.* Temperature compensated refractive-index sensing using a single Bragg grating in an abrupt fiber taper // IEEE Photonics J. 2013. V. 5. № 2. P. 7100208.

13. *Tsigaridas G., Polyzos D., Loannou A., Fakis M., Persephonis P.* Theoretical and experimental study of refractive index sensors based on etched fiber Bragg gratings // SENSOR ACTUAT A-PHYS. 2014. V. 209. № 9. P. 9–15.

14. *Wu Q., Semenova Y., Yan B., Ma Y., Wang P., Yu C., Farrell G.* Fiber refractometer based on a fiber Bragg grating and single-mode-multimode-single-mode fiber structure // Opt. Lett. 2011. V. 36. № 12. P. 2197–2199.

15. *Zhou K., Yan Z., Zhang L., Bennion I.* Refractometer based on fiber Bragg grating Fabry–Perot cavity embedded with a narrow microchannel // Opt. Express. 2011. V. 19. № 12. P. 11769–11779.

16. *De-Wen Duan, Yun-Jiang Rao, Lai-Cai Xu, Tao Zhu, Di Wu, Jun Yao.* In-fiber Mach–Zehnder interferometer formed by large lateral offset fusion splicing for gases refractive index measurement with high sensitivity // SENSOR ACTUAT B-CHEM. 2011. V. 160. № 1. P. 1198–1202.

17. *Lu P., Men L., Sooley K., Chen Q.* Tapered fiber Mach–Zehnder interferometer for simultaneous measurement of refractive index and temperature // Appl. Phys. Lett. 2009. V. 94. № 13. P. 131110–131110-3.

18. *Xiao-Yan Sun, Dong-Kai Chu, Xin-Ran Dong, Chu-Zhou, Hai-Tao Li, Luo-Zhi, You-Wang Hu, Jian-Ying Zhou, Cong-Wang, Ji-An Duan.* Highly sensitive refractive index fiber inline Mach–Zehnder interferometer fabricated by femtosecond laser micromachining and chemical etching // Optics & Laser Technology. 2016. V. 77. № 11. P. 11–15.

19. *Wang J.N., Tang J.L.* Photonic crystal fiber Mach–Zehnder interferometer for refractive index sensing // Sensors. 2012. V. 12. № 3. P. 2983–2995.

20. *Wang P., Semenova Y., Wu Q., Farrell G., Ti Y., Zheng J.* Macrobending single-mode fiber-based refractometer // Appl. Opt. 2009. V. 48. № 31. P. 6044-9.

21. *Mishra S.K., Varshney C., Gupta B.D.* Sensitivity enhancement of a surface plasmon resonance based fiber optic refractive index sensor utilizing an additional layer of zinc oxides // SENSOR ACTUAT A-PHYS. 2013. V. 193. № 5. P. 136–140.

22. *Zynio S.A., Samoylov A.V., Surovtseva E.R, Mirsky V.M., Shirshov Y.M.* Bimetallic layers increase sensitivity of affinity sensors based on surface plasmon resonance // Sensors. 2002. V. 2. № 2. P. 62–70.

23. *Jieyuan Tang, Junjie Zhou, Junwen Guan, Shun Long, Jianhui Yu, Heyuan Guan, Huihui Lu, Yunhan Luo, Jun Zhang, Zhe Chen.* Fabrication of side-polished single mode-multimode-single mode fiber and its characteristics of refractive index sensing // IEEE J. Sel. Top. Quan. 2016. V. 23. № 2. P. 5600708.

24. *Alvare-Herrero A., Guerrero H., Levy D.* High-sensitivity sensor of low relative humidity based on overlay on side-polished fiber // IEEE Sens. J. 2004. V. 4. № 1. P. 52–56.

25. *Yan Lu, Wang Guan-jun, An Yong-Quan, Wang Zhi-bin, Gui Zhi-guo.* Research on transmission character of side polished fiber // Journal of Measurement Science Instrumentation. 2016. V. 7. № 2. P. 145–148.

26. *Zhong Y., Li S., Tang L., Chen Z., Yu J.* High-sensitivity optical sensing of temperature based on side-polished fiber with polymer nanoporous cladding // Opt. Eng. 2016. V. 55. № 10. P. 106123.

27. *Yaoming Huang, Wenguo Zhu, Zhibin Li, Gguanglei Chen, Liheng Chen, Junjie Zhou, Hai Lin, Junwen Guan, Wwenxiao Fang, Xin Liu, Huazhou Dong, Jieyuan Tang, Heyuan Guan, Huihui Lu, Yi Xiao, Jun Zhang, Hongcheng Wang, Zhe Chen, Jianhui Yu.* High-performance fiber-optic humidity sensor based on a side-polished fiber wavelength selectively coupled with grapheme oxide film // Sensor. Actuat. B-Chem. 2018. V. S0925-4005. № 17. P. 31464-8.

28. *Xiaoli He, Zhe Chen, Jianhui Yu, Yingxin Zeng, Yunhan Luo, Jun Zhang, Jieyuan Tang, Huihui Lu.* Numerical analysis of optical propagation characteristics of side-polished photonics crystal fiber // OQE. 2014. V. 46. № 10. P. 1261–1268.

29. *Müller-Kirsten H.J.* Introduction to quantum mechanics: Schrödinger Equation and path integral. Singapore: World Scientific, 2012. 325 p.

30. *Winitzki S.* Cosmological particle production and the precision of the WKB approximation // PhRvD. 2007. V. 72. № 10. P. 10411.